Initial Results of Radio Occultation Observations of Earth's Atmosphere using the Global Positioning System (GPS)

E. R.Kursinski*[1,2], G. A. Hajj[2], W.I.Bertiger[2], S. S.Leroy[2], T.K.Meehan[2],
L. J. Romans[2], J. T. Schofield[2], D. J. McCleese[2], W. G. Melbourne[2], C. L. Thornton[2],
T.P.Yunck[2], J. R.Eyre[3], R.N.Nagatani[4]

[1]Division of Geological and Planetary Sciences, California Institute of Technology.

[2]Jet Propulsion Laboratory, California Institute of Technology.

[3]United Kingdom Meteorological Office.

[4]National Meteorological Center (NMC).

September 4, 1995

Revised: December 8,1995

submitted to SCIENCE

Recent radio occultation measurements using Global Positioning System satellite transmitters and an orbiting receiver have provided a globally distributed set of accurate, high resolution atmospheric profiles, suggesting that the technique should make a major contribution to global change and weather prediction programs. Biases in occultation temperatures relative to radiosonde and model data are ~1 Kelvin or less in the tropics and generally less than 0.5 Kelvin at higher latitudes. Data quality is sufficient to quantify significant model errors in remote regions. Temperature profiles also reveal an equatorial Rossby-gravity wave. Such waves provide a fundamental source of momentum for the stratospheric circulation.

Radio occultation is a technique for sounding the structure of atmospheres from space with high accuracy and vertical resolution. Since the mid-1960's, it has been employed by planetary

spacecraft to measure vertical density, pressure and temperature structure in the atmospheres of Venus, Mars, and the outer planets *(1-5)*. With the completion of the constellation of 24 orbiting radio transmitters known as the Global Positioning System (GPS), the sensitivity and coverage necessary to improve upon existing data sets for the Earth's atmosphere in a simple, cost effective manner are now available. Here we present initial temperature and water vapor profile data derived from measurements made in April and May 1995 during the prototype GPS occultation mission, GPS-MET, launched in April 1995 *(6)*. These profiles are compared with radiosonde (balloon) data and atmospheric analyses available every 6 hours from the European Center for Medium-range Weather Forecasts (ECMWF) *(9,10)*. A comparison made between about 150 retrieved temperature profiles in the northern hemisphere and the ECMWF analysis, indicates that, between 5 and 30 km altitude, GPS occultation temperature profiles are accurate to better than 1 K in the mean with a standard deviation of 1-2 K, Theoretical predictions suggest that GPS radio occultation is capable of< 1 K accuracy below 35 km, with a vertical resolution of< 1 km , and a horizontal resolution of< 200 km, and is insensitive to clouds and aerosols *(11,12,13)*. With a potential S00 occultations per day per orbiting receiver, the technique provides a unique combination of well distributed global coverage and high vertical resolution currently unobtainable, particularly in the troposphere, from either the land-biased radiosonde network or space-based sensors.

In radio occultation, the atmosphere acts as a planetary-scale lens. Signals from a transmitter which pass through the atmosphere are deflected by the vertical gradient of atmospheric refractive index and then detected by an orbiting receiver (Fig. 1). Bending angle, α, varies with impact parameter, a, as the orbital motion of the transmitter and receiver cause the tangent height of the raypath to descend through the atmosphere. The vertical refractive index profile, n(r), is derived from measurements of $\alpha(a)$ using an Abel integral transform, subject to the assumption of local spherical symmetry *(1)*. Temperature profiles are obtained from n(r) using empirical data on the variation of refractive index with atmospheric properties *(14)*. Bending angle, $\alpha(a)$, is

calculated from receiver measurements of the Doppler frequency of the occulted beam, given precise knowledge of the positions and velocities of the transmitter and receiver *(15)*.

Below 90 km, the primary contributors to radio wavelength refractivity, defined by $N(r)=[n(r) - 1] \times 10^6$, are dry atmospheric density and water vapor density. Throughout the middle atmosphere and the regions of the troposphere colder than 250 K, the contribution of water vapor to refractivity is small and measured refractivity profiles can be converted directly to density profiles which are then integrated hydrostatically to determine pressure. Given density and pressure, temperature is obtained from the ideal gas law. Temperature errors due to 50% uncertainties in climatological water vapor at the 250 K level are less than 1 K *(12,18,19)*. Based on noise considerations, the hydrostatic integral is initialized at 50 km in the temperature retrievals presented below, and a temperature estimate at 50 km is required as a boundary condition. This temperature, derived from a model, is the only independent atmospheric information used in the retrieval process when the atmosphere is dry. A 10 K error in the 50 km temperature estimate produces a temperature error of approximately 0.1 K at the 100 mbar level (-16 km).

Retrieved occultation temperature profiles can be evaluated by comparing specific examples with radiosonde and ECMWF model profiles (Fig. 2). At high latitudes, cold, dry conditions allow accurate temperatures to be derived almost to the surface (Fig. 2a). The retrieved profile is similar to the nearby radiosonde profile, with differences of order 1 K through most of the troposphere. In the vicinity of the tropopause and above, temperature differences are comparable to those between the radiosonde and model analysis. Agreement with the radiosonde in resolving the sharply defined tropopause and the lapse rate change below 3 km is illustrative of the sensitivity and vertical resolution of the occultation technique, At low latitudes, the ability of the technique to measure the high and cold tropopause structure characteristic of the tropics is illustrated (Fig 2b). Figure 2b also illustrates the sensitivity of radio occultation to atmospheric waves (4,20,21,22). Waves are most apparent in the equatorial lower stratosphere, Although other waves are present

throughout this region, one of ~ 3 km vertical wavelength appears in a number of profiles within 10 degrees of the equator above the Pacific with a vertical structure antisymmetric about the equator. Close agreement in both amplitude and phase with a radiosonde sounding taken some 300 km away (Fig, 2b) implies that the wave has been resolved by the occultation measurement and that the horizontal wavelength is large (>> 300 km). These features, the wave's absence in a profile at 0,30 north latitude, and an amplitude which has largely decayed by the 10 mbar level (~30 km) are consistent with a 4 to 5 day westward propagating Rossby-gravity wave, one of the two dominant wave types observed previously in this region (the other is a 10 to 20 day Kelvin wave) *(23)*. These waves maybe generated by tropical convection and provide significant sources of energy and momentum for the stratospheric circulation. 'J'he location of the wave is consistent with a convective source over the warm pool region around Indonesia,

As temperatures rise above 250 K lower in the troposphere, water concentrations increase dramatically. This introduces an ambiguity in the interpretation of refractivity but also allows water vapor to be retrieved given independent temperature data (Fig. 3) (19,24,25,26). The retrieved water vapor in Figure 3 is biased high by 0.1 to 0.4 mbar relative to the radiosonde due to systematic differences between the retrieved and radiosonde refractivity profiles. Biases of a similar magnitude are expected at low latitudes giving relative accuracies an order of magnitude better. Unfortunately, the vertical structure often associated with higher water concentrations at lower latitudes causes large variations in the occulted signal which the GPS-MET receiver can not adequately track. Results for temperatures warmer than 250 K are therefore not generally presented here. Receiver modifications to improve low altitude signal tracking are in progress. At low latitudes, the vertical resolution, insensitivity to clouds and coverage of GPS occultations are needed to address fundamental issues in hydrology, weather and climate, and are lacking in present satellite sensors (27).

To evaluate the accuracy of our temperature profiles, given the rarity of close coincidences with radiosondes, we have compared them with the ECMWF analyses (Fig. 4). Tropospheric temperatures exceeding 250 K were excluded from the comparisons. In the northern hemisphere troposphere, where the ECMWF analyses are the most accurate, mean temperature differences arc generally less than 0.5 K and the standard deviations of the differences are of order 1 K. These differences include vertical structure that is not resolved by the ECMWF analysis, especially above the 100 mbar level,

Although radiosonde and TIROS Operational Vertical Sounder (TOVS) (28) data are assimilated into the ECMWF model, the analyses are less accurate in some regions of the southern hemisphere due to the sparse distribution of radiosondes. Greater knowledge of the structure of the atmosphere over the southern hemisphere oceans is essential for studies of climate and the global energy and water cycles. As the occultation retrieval process has little dependence on latitude, these temperature measurements can be used to characterize atmospheric structure in the southern hemisphere in more detail. In the southern hemisphere, mean temperature differences and standard deviations increase at lower altitudes (Fig. 4c). This feature is produced by 12 occultation profiles which are concentrated far from radiosonde ascents, primarily in the southeastern Pacific in the southern hemisphere storm track and close to the ice edge, where problems in the assimilation of TOVs data are known to arise (29). The statistics for these 12 profiles when compared with those of the remaining 38 southern hemisphere profiles, reveal a bimodal signature in model accuracy (Fig. 5). Biases and standard deviations of the temperature differences of the 38 profiles (Fig. 5a) arc generally comparable to those in the northern hemisphere (Fig. 4a). In contrast, the 12 profiles (Fig. 5b) show that the model tropopause altitude is 1-2 km too low, and model temperature is ~2 K too low in the troposphere and ~3 K too high in the lower stratosphere. These differences are larger than the predicted decadal climate variations and imply that caution is appropriate when using model data to establish climatological behavior and study climatic changes in regions devoid of high vertical resolution observations. The temperature biases and errors in

tropopause height, which must be significant given the importance of the height and topography of the tropopause to tropospheric dynamics (30), suggest that GPS occultation measurements will improve medium range weather forecasts in regions where weather systems move from remote oceans onto continents.

Temperature differences at tropical latitudes also display distinctive structure (Fig. 4b). On average, retrieved profiles are colder than the ECMWF analyses between 300 and 70 mbar, with a maximum difference of about 1 K near 150 mbar whereas above the 70 mbar level, they become warmer by a similar amount. Retrieved temperature gradients between 80 and 60 mbar are therefore systematically larger than model gradients. Although a little warmer than the retrievals, radiosonde data exhibit similar temperature structure in this altitude range suggesting that the model does not have sufficient resolution to represent these gradients. As equatorial waves in the lower stratosphere are not resolved by the model, they are probably responsible for the increase in standard deviation above the 100 mbar level in Figure 4b.

The source of the temperature biases in the upper tropical troposphere (Fig. 4b) is not understood. These biases could affect convective available potential energy in the troposphere, and therefore energy transfer within the atmosphere and the severity of convective storms. They could also affect radiative emission by cirrus clouds, an important component of the greenhouse effect, and troposphere-stratosphere exchange through the thermal control of water vapor transfer. Given the preliminary nature of these results, the biases seen in Figure 4b could be due to occultation measurement error, However, the good agreement between the retrievals and model in the northern hemisphere (Fig. 4a) argues against this. Errors in the model data are due primarily to incomplete model physics and imperfect radiosonde observations, Model physics becomes important when the model extrapolates to locations and times far from the ground truth provided by radiosondes. However, radiosonde temperatures are themselves imperfect and require corrections for absorption of solar and IR radiation, thermal emission, and conduction and convection of heat

(31). Inadequate calibration could contribute to the temperature biases seen in Figure 4b, to the extent that the model is constrained by radiosondes in this region,

Figures 2,3,4 and 5 indicate that future measurements, if available in near real-time, could play a significant role in numerical weather prediction (NWP). The density of 500 globally-distributed measurements per day provided by a single orbiting GPS receiver would exceed that of the radiosonde network by a factor of two in the southern hemisphere, making a significant contribution to the global observing system. A constellation of orbiting receivers could make a major contribution to fulfilling the stated temperature observation requirements for global NWP. The results presented in this paper have demonstrated desirable properties for use in NWP namely generally good agreement with a high-quality NWP analysis, plus the ability to identify a minority of cases where there is room for significant improvement in the analysis.

References and Notes

1. G.F.Fjeldbo, V. R. Eshleman and A. J. Kliore, *Astronom. J.,* 76, 123 (197 1).

2. G. F.Lindal, *J. Geophys. Res..,* 84, 8443 (1979).

3. A. J. Kliore and I. R. Patel, *J. Geophys. Res.,* 85, 7957 (1980).

4. D. P.Hinson and J. A. Magalhaes, *Icarus,* 94,64 (1991).

5. G.F.Lindal, *Astronom. J., 103, 967 (1992).*

6. Atmospheric radio occultation observations using a GPS receiver in low earth orbit were proposed and developed for NASA'S Earth Observing System in 1988 (7), but the concept became a reality with the launch of the University Corporation for Atmospheric Research (UCAR) GPS-MET experiment on April 3rd, 1995 (8).

7. T. P. Yunck, G.F.Lindal and C.H.Liu, *Proc. of IEEE Pos., Lot., and Nav. Symp.,* Orlando FL, 251 (1988).

8. R.Ware *et al., Bull. Amer. Met. Sot.* Submitted (1995).

9. A. C. Lorenc, *Mon Weather Rev, 109, 701 (1981).*

10. D.B.Shaw, P.Lonnberg, A.Hollingsworth and P. Unden, *Quart. J. R. Met. Sot., 113,* **533 (1987).**

11. E. R. Kursinski, G. A.Hajj and K, R.Hardy, *Proc. of 8th Symp. on Meteorological Observations and Instrumentation, Am. Met. Sot.,* J 153 (1993).

12. E. R.Kursinski, G. A.Hajj and K.R.Hardy, *Proc. of SPIE Symp. on Optical Engineering and Photonics in Aerospace Science and Sensing,* Paper No. 1935-13 (1993).

13. K. R. Hardy, G. A. Hajj and 1% R. Kursinski, *Intern. J. Sat. Comm., 12, 463 (1994).*

14. *G. D.Thayer, Radio Sci., 9, 80 (1974).*

15. *To* obtain the accuracies necessary for atmospheric work, we have used a modified version of the GIPSY-OASIS II system developed at the Jet Propulsion Laboratory (JPL) for the Ocean Topography Experiment (TOPEX/Poseidon) to determine receiver and transmitter orbits, and to calibrate and remove receiver and transmitter clock biases and instabilities *(13,16).* Vertical smoothing, decreasing from -1.4 km in the stratosphere to -0.5 km near the surface, has also

been applied to the Doppler frequency measurements to make them consistent with the Fresnel diffraction resolution limit (4,11). Finally, unwanted dispersive ionospheric contributions to bending are removed by forming a linear combination of the bending angles estimated independently for each of the two GPS signal frequencies (17).

16. Bertiger, W. I, et al., *J. Geophys. Res.,* 99, 24449 (1994),

17. Vorob'ev, V.V. and Krasil'nikova, T.G. *Izvestia A N. Fizica Atmosfery i Okeana*, 29, 626 (1993)₀

18. G. A.Hajj, E.R.Kursinski, W.I.Bertiger, L.J.Remans and K. R.Hardy, *Proc. of 7th Conf. on Sat. Meteorology and Oceanography , Am, Met. Sot.,* J7 *(1994).*

19. 13. R. Kursinski, G. A.Hajj, K. R.Hardy, L.J.Remans and J. T. Schofield, *Geophys. Res. Lett.*, 22, 2365 (1995).

20, D.P.Hinson and G.L.Tyler, *Icarus,* 54,337 (1983).

21. D.P.Hinson and J. A. Magalhaes, *Icarus,* 105, 142 (1993).

22. D.P.Hinson and J. M. Jenkins, *Icarus, 114,* **310 (1995).**

23. D. G. Andrews, J.R.Holton and C.B.Leovy, *Middle Atmosphere Dynamics,* Academic Press, Orlando, FL (1987).

24. E.R.Kursinski, G.A.Hajj and K.R.Hardy, *Eos Trans. AGU ,72,* 372 (1991).

25. M. Bevis, *et al., J. Geophys. Res.,* 97, 15787 (1992).

26. L.L.Yuan, et *al., ibid, 98, 14925 (1993).*

27. D.O'C. Starr and S.H.Melfi, NASA Conference Publication 3120, May (1991).

28. W.L.Smith, H.M.Woolf, C.M.Hayden, D. Q. Wark, and L, M, McMillan, *Bull. Amer. Met. Sot. ,60,* 1177 (1979).

29. J. R. Eyre, G. A. Kelly, A. P. McNally, E. Andersson and A. Persson, *Quart. J. R. Met. Sot.,* **119,** 1427 (1993).

30. B. J.Hoskins, M.E. McIntyre and A.W. Robertson, *ibid, 111,* 877 (1985).

31. J. K. Luers and Eskridge, R. E., *J. Appl. Met.,* 34, 1241 (1995).

Figure Captions

FIG 1. Schematic of the low earth orbiter (LEO) GPS occultation geometry of GPS-MET, defining the occultation bending angle, α, the impact parameter, a and the radius to the ray periapsis tangent point, r.
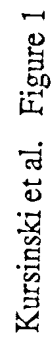
FIG 2. Comparisons between occultation, radiosonde, and ECMWF temperature profiles. The left panel compares the profiles and the right panel displays temperature differences (Occultation - Radiosonde/Model) as a function of altitude. (a). Occultation obtained at 01:33 UT on 5th May, 1995 over Hall Beach, Northwest Territories, Canada (69.2°N, 82.6°W). The radiosonde (00 hr UT, 68.8°N, 81.3°W) is 65 km from the occultation location, and the model analysis from 00 UT is spatially interpolated to the occultation location. (b). Occultation obtained at 12:40 UT on 4th May, 1995 in the south Pacific (7.90S, 167.5°E). The radiosonde profile (12 hr UT, 6.0°S, 170.4°E), obtained from a ship, is 350 km from the occultation location and the model analysis from 12 hr UT is spatially interpolated to the occultation location. Thick solid line is the retrieval, the thin solid line is the radiosonde and the dotted line is the ECMWF analysis.
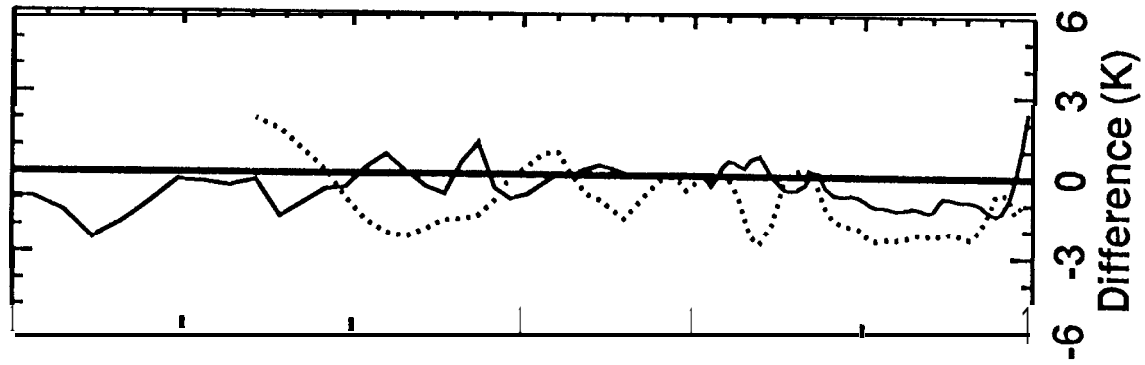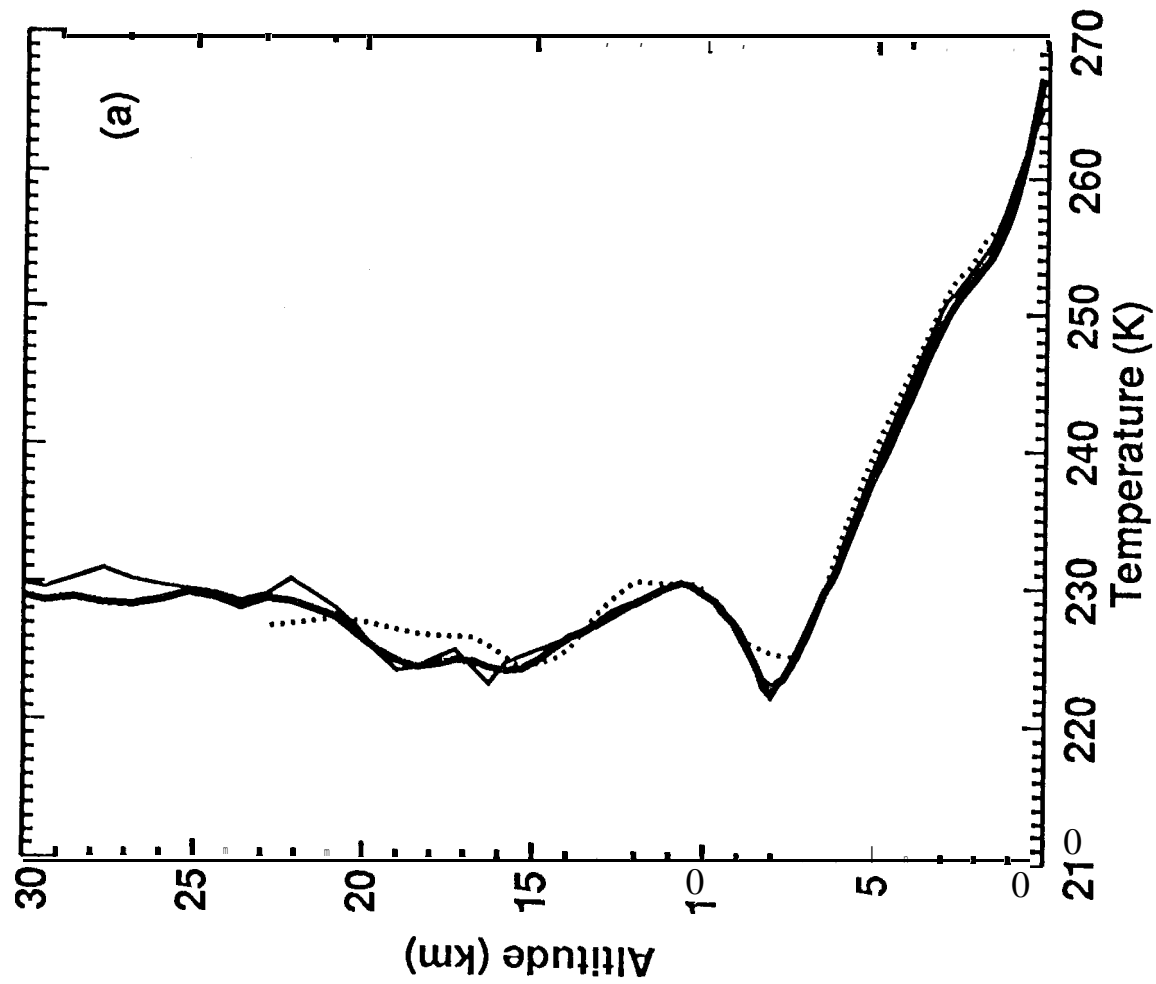
FIG 3. Comparison between the occultation and radiosonde water vapor profiles for the occultation over Hall Beach (Fig.2a). Solid curve is occultation, dashed curve radiosonde The radiosonde temperature profile is used to remove the dry density contribution from the occultation refractivity profile in order to isolate the water vapor component. The water vapor retrieval is initialized at about 6.2 km altitude where water vapor abundance is assumed to be zero.

FIG 4. Statistical comparisons between the 6 hour ECMWF analyses and temperature profiles retrieved from radio occultations on 4th and 5th May, 1995. The panels plot mean temperature differences (retrieved-ECMWF) for (a) 54 profiles in the northern hemisphere (> 30°N), (b) 52 profiles in the tropics (30°S to 30°N), and (c) 50 profiles in the southern hemisphere (> 30°S). The vertical curve represents mean temperature differences and the horizontal error bars depict the

standard error in the mean. The shaded area is defined by the mean temperature difference plus or minus the standard deviation of the temperature difference about the mean. In the northern and southern hemispheres, the troposphere-stratosphere boundary (tropopause) typically lies in the 250 to 300 mbar range, whereas in the tropics it is near the 100 mbar level.

FIG 5. Statistical comparison of the 50 southern hemisphere profiles divided into two groups: (a) 38 profiles which differ little relative to the model and (b) 12 profiles with the largest deviations relative to the model,
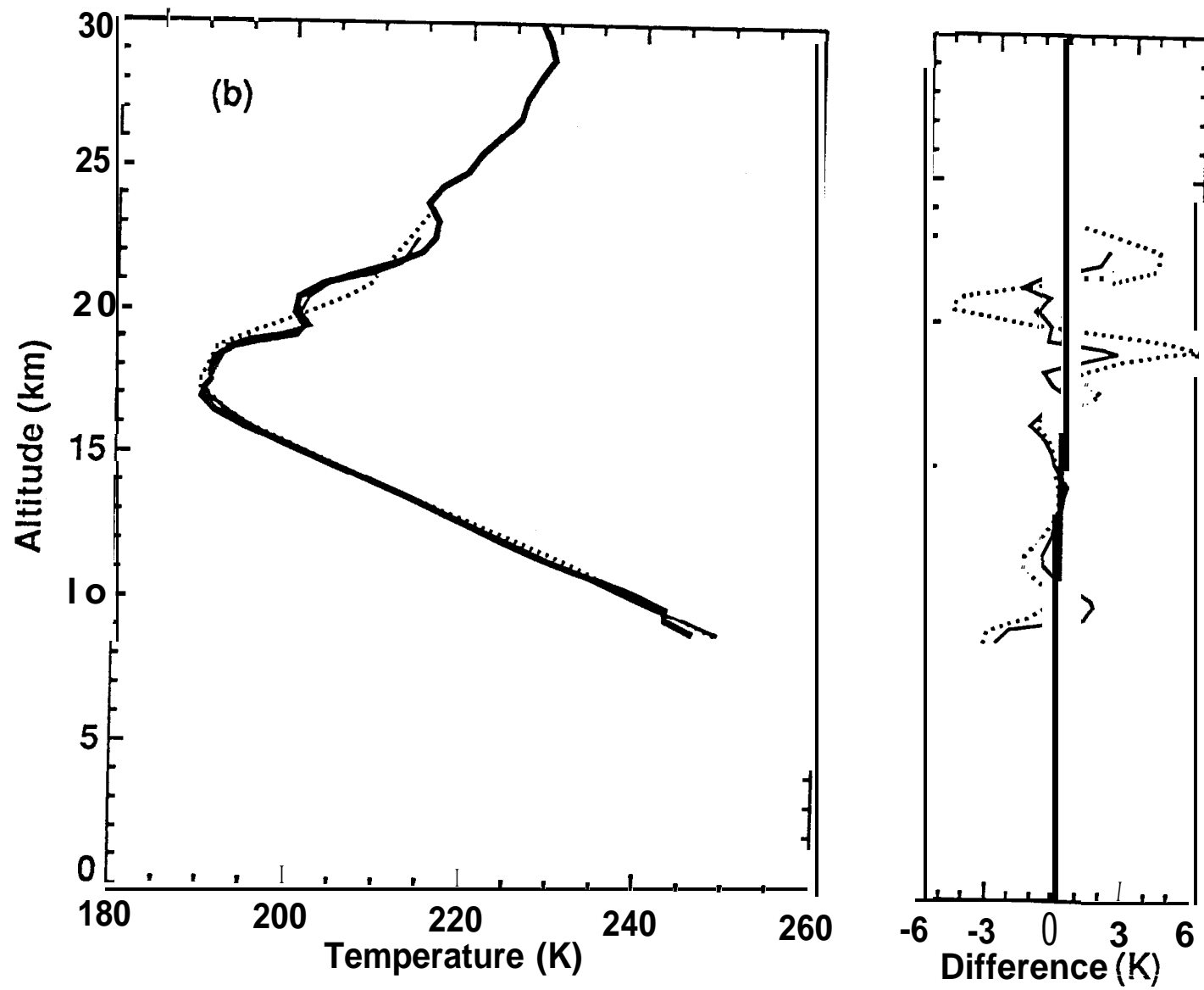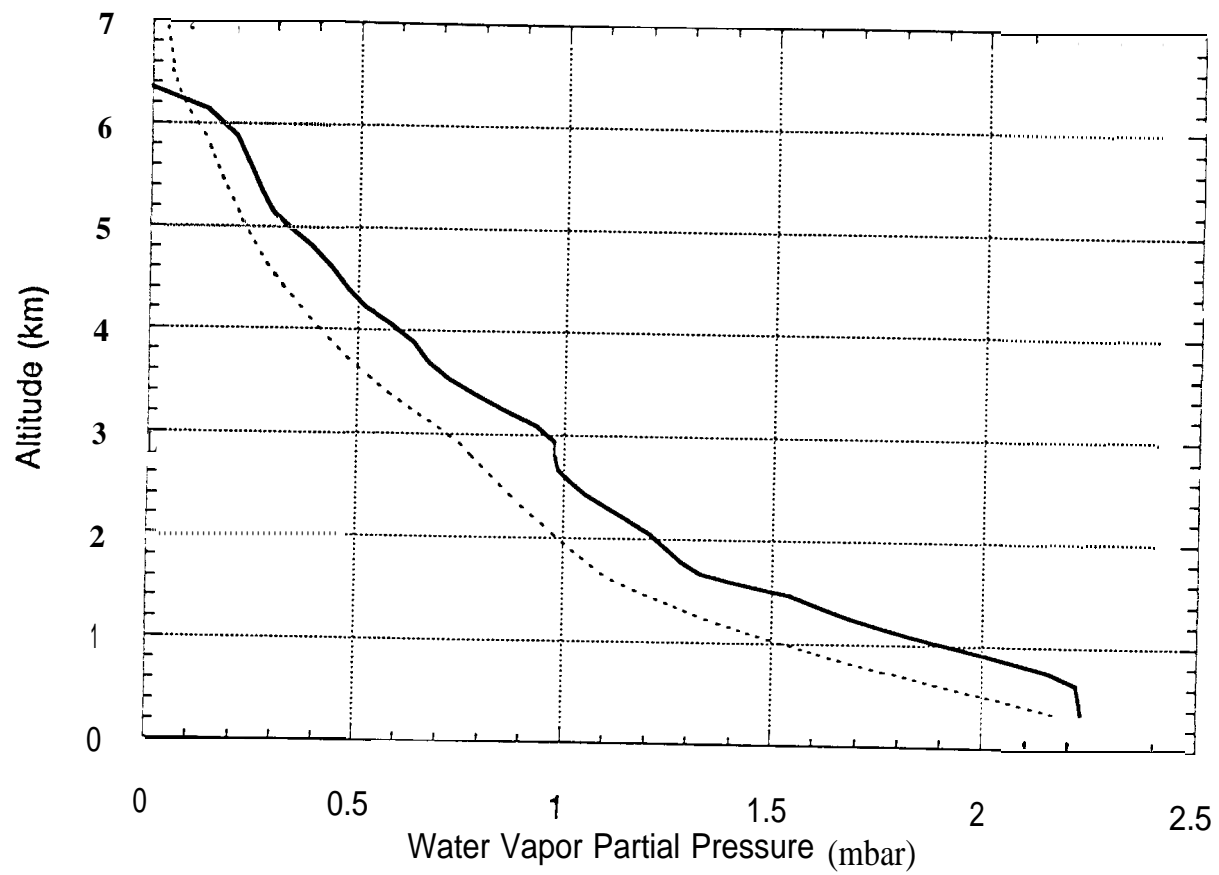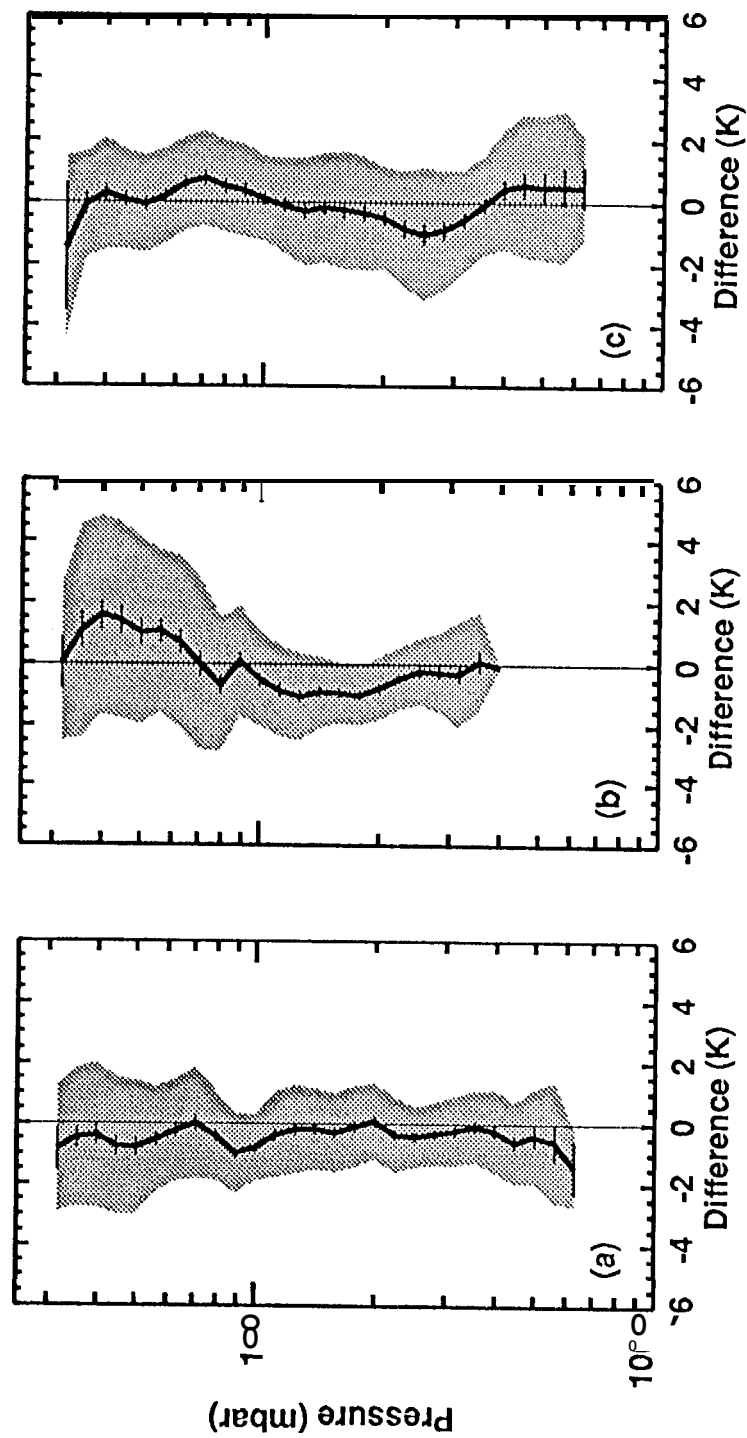
GPS

Tangent Point

α

r

a

a

Earth

LEO

Kursinski et al.   Figure 1

Figure 2a

Figure 2b

Figure 2

Figure 4

Figure 5